

Analysis of dilute phase pneumatic conveying through pipe systems by the Euler/Lagrange approach

Martin Sommerfeld^{1,2} and Santiago Lain²

¹ Zentrum für Ingenieurwissenschaften, Martin-Luther-Universität Halle-Wittenberg, D-06099 Halle (Saale), Germany

² Universidad Autónoma de Occidente, Department of Mechanical Engineering, Cali, Columbian

*Corresponding author, E-mail address: martin.sommerfeld@iw.uni-halle.de

ABSTRACT

The present contribution summarises research related to the numerical computation of pneumatic conveying systems applying the Euler/Lagrange approach. For that purpose a rigorous modelling of the particulate phase was aspired, including the relevant fluid dynamic forces, particle wall collisions with wall roughness and inter-particle collisions. For the validation of the computations experiments of Huber and Sommerfeld (1994) were selected for the conveying through an 80 mm stainless steel pipe with 5 m horizontal pipe, bend and 5 m vertical pipe. The majority of the computations were done for the same pipe system, however consisting of 150 mm stainless steel pipes. For this configuration the influence of wall roughness, inter-particle collisions, particle size and mass loading on the resulting particle concentration distribution, the secondary flow as well as the pressure drop was analysed. Moreover, a segregation parameter was defined which describes the location of the maximum particle concentration throughout the pipe system. Eventually, also the rope formation in a horizontal pipe, a pipe bend and another horizontal pipe was analysed.

INTRODUCTION

Particle-laden confined flows are widely found in the processing industries. Typical examples are pneumatic conveying within processes, pneumatic mixing devices and particle separation equipment, typically represented by gas cyclones. An experimental design and lay-out of such equipment is rather cumbersome, since numerous parameters and elementary processes are affecting the performance. In dilute-phase pneumatic conveying these are (Siegel 1991): pipe configuration, diameter and wall material; particle material, shape and size distribution and of course particle mass loading.

Therefore, the Euler/Lagrange approach was further developed over the last decades for allowing a reliable numerical prediction of such confined flows. This approach is most suitable for the calculation of such processes since a particle size distribution has to be considered and particle-wall collisions are dominantly affecting these processes and hence integral properties such as pressure drop and grade efficiency curves. The developed wall collision model accounts for wall roughness effects through a stochastic treatment using a pre-defined standard deviation of the wall roughness angle distribution which is correlated with the particle size

(Sommerfeld 1992, Sommerfeld and Huber 1999, Sommerfeld and Lain 2009). As even at low overall mass loading with volume fractions around $\sigma_p = 10^{-3}$ the inertial segregation of particles due to gravity and centrifuging effects yields locally rather high particle concentrations inter-particle collisions will become of importance, resulting in a re-distribution of the particle phase (Sommerfeld 1998). A deterministic inter-particle collision model is numerically rather elaborate since the detection of collisions requires $N_p(N_p - 1)/2$ checks for possible collisions. In order to achieve high computational efficiency, the stochastic inter-particle collision model has been developed where fictitious collision partners are generated based on the local particle phase properties at each time step of real particle tracking (Sommerfeld 2001). Naturally, the effect of the particles on the fluid flow is important in the applications considered, especially in regions of strong segregation. This is realised by particle phase source terms in the momentum equations and the transport equations of the turbulence properties, in this case the turbulent kinetic energy and the dissipation rate. Hence, the computations are done fully four-way coupled using under-relaxation for improving convergence behaviour of the applied hybrid approach (Kohnen et al. 1994). The convergence behaviour for two-way and four-way coupling was clearly demonstrated for a particle-laden channel flow (Lain and Sommerfeld 2012 a). For validating the numerical computations of pneumatic conveying in a horizontal pipe and the vertical pipe behind the bend the experiments of Huber and Sommerfeld (1994, 1998) performed in a system with either glass or stainless steel pipes with 80 mm and 150 mm diameter are considered. The experiments were conducted with spherical glass beads having a size distribution between 15 and 85 μm . All measurements were performed by phase-Doppler anemometry (PDA) allowing also the determination of local particle size distributions as well as profiles of the particle number mean diameter, documenting the effect of particle size segregation in horizontal pipes and bends. In addition particle concentration or mass flux profiles as well as particle velocity profiles were compared. A reasonable good agreement was obtained for all properties, indicating the proper performance of the involved models (Lain and Sommerfeld 2010; 2012 b). Moreover, the conveying characteristics were analysed by considering global properties, such as pressure drop, degree of particle segregation and secondary flow modification. Thereby, the influence of different effects, such as degree of wall

roughness, pipe diameter, particle mass loading, particle size distribution and conveying velocity, on pneumatic conveying through the pipe system were thoroughly studied (Lain and Sommerfeld 2009, 2010, 2011, 2012 c). The present contribution summarises numerical results where the influence of several parameters and elementary process on the performance of pneumatic conveying systems was analysed.

EULER/LAGRANGE-APPROACH

The numerical scheme adopted to calculate the considered particle-laden two-phase flows was the fully coupled Euler/Lagrange approach (Lain and Sommerfeld 2008). The fluid flow was calculated based on the Euler approach by solving the Reynolds-averaged conservation equations in connection with the standard k - ε turbulence model. All conservation equations were extended in order to account for the effects of the dispersed phase, i.e., two-way coupling. The time-dependent three-dimensional conservation equations for the fluid may be written in the general form (using tensorial notation) as:

$$(\rho\phi)_{,t} + (\rho U_i \phi)_{,i} = (\Gamma_{ik} \phi_{,k})_{,i} + S_\phi + S_{\phi p} \quad (1)$$

where ρ is the gas density, U_i are the Reynolds-averaged velocity components, and Γ_{ik} is an effective transport tensor. The usual source terms within the continuous phase equations are summarised in S_ϕ , while $S_{\phi p}$ represents the additional source term due to phase interaction, i.e. the influence of the particles on the fluid flow (see Lain and Sommerfeld 2008). In the present study, the computations have been done for a stationary flow situation.

The simulation of the particle phase by the Lagrangian approach is based on tracking a large number of particles through the beforehand computed flow field. Particles are treated as point masses and their shape is assumed to be spherical. In order to account for the correct particle mass flow rate, the considered computational particles represent a certain number of real particles with the same properties, which yields a computationally treatable number of parcels. Tracking requires the solution of the equations of motion for each computational particle or parcels. The forces which were considered include particle inertia, drag, gravity/buoyancy, slip-shear lift force F_{ls} and slip-rotational lift force F_{lr} . The Basset history term, the added mass and the fluid inertia are negligible for the considered high ratio of particle to gas densities. The change of the angular velocity along the particle trajectory due to the viscous interaction with the fluid (i.e. the torque T_i) requires the solution of an additional partial differential equation. Hence, the complete equations of motion for the particles are given by:

$$\frac{dx_{pi}}{dt} = u_{pi} \quad (2)$$

$$m_p \frac{du_{pi}}{dt} = \frac{3}{4} \frac{\rho}{D_p} m_p c_D (u_i - u_{pi}) \left| \vec{u} - \vec{u}_p \right| + m_p g_i \left(1 - \frac{\rho}{\rho_p} \right) + F_{lsi} + F_{lri} \quad (3)$$

$$I_p \frac{d\omega_{pi}}{dt} = T_i \quad (4)$$

where x_{pi} , u_{pi} and u_i are the components of the particle location vector and the particle and fluid velocity,

respectively. Furthermore, m_p is the particle mass, I_p the moment of inertia, D_p the particle diameter, g_i the gravity vector and ρ and ρ_p are the fluid and particle material densities. The different forces acting on the particles and the respective resistance coefficients allowing the extension of the equation of motion to higher particle Reynolds numbers are presented by Sommerfeld et al. (2008) as well as Lain and Sommerfeld (2008), Lain and Sommerfeld (2012 c) and therefore not repeated here. For solving the partial differential equations (Eq. 2-4) a dynamic time step is used which is automatically adjusted according to the local restricting time scales such as particle response time, integral time scale of turbulence and inter-particle collision time.

Two-way coupling considers the momentum transfer from the dispersed phase to the continuous phase and vice versa through appropriate source terms in the momentum equations and the conservation equations of turbulent kinetic energy and the dissipation rate. The source terms are accumulated for each control volume during the Lagrangian tracking procedure. An under-relaxation approach is used when introducing the source terms in the conservation equations of the fluid flow (for details see Kohnen et al. 1994 and Lain and Sommerfeld 2012 a). Hence, a sequential calculation of fluid flow and particle phase is performed until the coupled hybrid system has converged. For the present calculations typically about 25 to 55 coupling iterations with an under-relaxation factor between 0.1 and 0.5 were necessary in order to yield convergence of the Euler-Lagrange coupling.

MODELLING OF ELEMENTARY PROCESSES

In order to account for turbulence effects on particle motion, the instantaneous fluid velocity components along the particle trajectory are determined from the local mean fluid velocity interpolated from the neighbouring grid points and a fluctuating component generated by a single-step isotropic Langevin model described by Sommerfeld et al. (1993). In this model the fluctuation velocity is composed of a correlated part from the previous time step and a random component drawn from a Gaussian distribution function. The degree of correlation depends on the turbulent particle Stokes number which is calculated using appropriate time and length scales of turbulence estimated from the k - ε turbulence model.

Especially in wall bounded flows, as considered here, the modelling of particle-wall collisions needs special consideration. The applied wall collision model, accounting for wall roughness, is described and validated in Sommerfeld and Huber (1999). The wall roughness seen by the particle is simulated assuming that the instantaneous impact angle is composed of the particle trajectory angle plus a stochastic contribution due to wall roughness, drawn from a normal distribution with a standard deviation $\Delta\gamma$ which depends on the structure of wall roughness and particle size (Sommerfeld 1992). Corresponding correlations for the restitution coefficient, the friction coefficient and the roughness angle are presented by Lain et al. (2002), which are depending on the particle impact angle. Regardless of particle size, the standard deviation of the roughness angle was assumed to be $\Delta\gamma = 10^\circ$ for all cases considered here.

Inter-particle collisions are modelled by the stochastic approach described in detail by Sommerfeld (2001). This model relies on the generation of a fictitious collision

partner at each time step of tracking a real particle and accounts for a possible correlation of the translational velocities of colliding particles in turbulent flows. As model parameters for particle-particle collisions the restitution coefficient has been taken to be constant with 0.9 and the static and dynamic friction coefficients were chosen to be 0.4.

CONVEYING PIPE CONFIGURATION

The considered configuration of the horizontal to vertical 90°-bend has an inlet horizontal pipe and an outlet vertical pipe, both 5 m in length. According to the configuration described in Huber and Sommerfeld (1994) and Huber and Sommerfeld (1998), the pipe diameters are $D = 0.08$ m and 0.15 m and the elbow radius is 2.54 times the pipe diameter (i.e. $R_{\text{bend}} = 0.203$ m and 0.381 m), and the mean conveying velocity is different for each of the cases (Table 1). These conditions yield the non-dimensional parameters summarised in Table 1, where the pipe Reynolds number and the Dean number of the bend are determined from:

$$\text{Re}_{\text{pipe}} = \frac{\rho D_{\text{pipe}} U_{\text{av}}}{\mu} \quad \text{De}_{\text{bend}} = \frac{\text{Re}_{\text{pipe}}}{\sqrt{R_{\text{bend}}/R_{\text{pipe}}}} \quad (5)$$

Pipe diameter	0.08 m	0.08 m	0.15 m
Bulk velocity	14 m/s	21 m/s	27 m/s
Mass loading	0.5	0.5	0.3
Re_{pipe}	74,667	112,000	270,000
De_{bend}	33,144	49,716	63,890

Table 1: Parameters and non-dimensional properties of pipe system (5 m horizontal, bend and 5 m vertical).

The considered fluid properties are: $\rho = 1.2$ kg/m³, $\mu = 18.0 \cdot 10^{-6}$ N s/m² (air at room temperature). The multi-block structured O-type grid is composed of 25 blocks with a total of 568,000 hexahedral control volumes to discretise the entire pipe system. This resolution was found to be sufficient for producing grid-independent results.

The particles considered in the numerical calculations for the standard cases (see Table 1) were spherical glass beads ($\rho_p = 2,500$ kg/m³) with the size distribution shown in Figure 1. The size distribution has a number mean diameter of 40 μm and is rather wide ranging from about 15 to 85 μm , which was discretised by 7 diameter classes of 10 μm width. It should be noted that the size of injected particles was sampled from a continuous cumulative distribution, yielding also a variation of particle size in a size class.

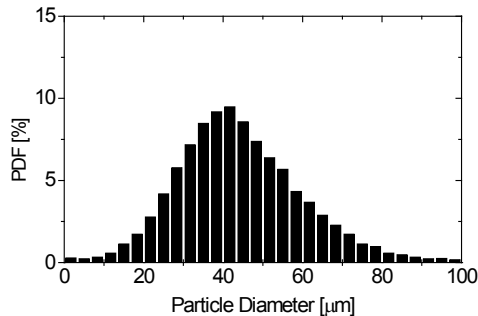


Figure 1: Size distribution of spherical glass beads (relative number frequency) used in the experiments of Huber and Sommerfeld (1998).

The particle mass loading [mass flow rate of particle/mass flow rate of air] for the standard cases was selected according to the experiments (Huber and Sommerfeld 1994; Huber and Sommerfeld 1998), see Table 1. Besides that, mono-sized particle with 40, 80 and 135 μm diameter and a binary mixture were considered (see Table 2), all being spherical glass beads with $\rho_p = 2,500$ kg/m³.

RESULTS HORIZONTAL TO VERTICAL PIPE

A particle-laden flow through a bend is characterized by strong segregation of the mixture, whereby the particles accumulated at the outer wall of the elbow due to inertial effects and a relatively dense rope is formed. This rope will be again disintegrated in the connecting vertical pipe due to inter-particle collisions, wall collisions, secondary flow and turbulence. The redirection of the two-phase flow from horizontal to vertical leads also, as a result of particles inertia, to enhanced wall collisions with the outer bend wall followed by a rebound towards the core of the pipe. The particle response behaviour regarding the mean motion through the bend is characterised by the bend Stokes number being the ratio of the particle response time (here the Stokesian response time is used) to the particle residence time along the centre line within the bend:

$$\text{St}_{\text{bend}} = \frac{\tau_p}{\tau_{\text{bend}}} = \frac{\rho_p d_p^2}{18 \mu C_{\text{bend},90^\circ}} \frac{U_0}{\pi R_{\text{bend}}} = \frac{\rho_p d_p^2}{18 \mu} \frac{2 U_0}{\pi R_{\text{bend}}} \quad (6)$$

Here $C_{\text{bend},90^\circ}$ is the arc of the 90° bend radius measured along the centre line, R_{bend} is the bend radius (2.54 times pipe diameter) and U_{av} is the average conveying velocity. The bend Stokes number for the different particle systems are also summarised in Table 2. Expectedly, an increase of this Stokes number is coupled with an increasing wall collision frequency, especially within the bend, and ultimately a growing pressure drop. The rebound characteristics of the particles are evidently affected by wall roughness and the involved shadow effect (Sommerfeld and Huber 1999).

Diameter [μm]	Turbulent Stokes ¹ [-]	Response distance [mm]	Bend Stokes ² [-]
① 15 – 85 (40)	0.169 – 5.412	0.03 – 30.49	0.078 – 2.515
② 40	1.199	1.5	0.557
③ 80	4.794	23.9	2.228
④ 135	13.653	194.0	6.344
⑤ 30 + 60 (40) ³	0.674 – 2.697	0.47 – 7.57	0.313 – 1.253

Table 2: Summary of particle response characteristics for the particle size distribution, different mono-sized particle and a binary mixture (¹ integral time scale of turbulence in the pipe core $T_L = 10.3$ ms; ² calculated according to Eq. 6 with $R_{\text{bend}} = 0.381$ m and $U_0 = 27$ m/s; ³ binary mixture with equal number of parcels and mass fractions of $w_{30} = 20$ % and $w_{60} = 80$ %, number mean diameter 40 μm).

The high particle concentration region developing within a bend is of course altering the probability if inter-particle collisions with the result that the distribution of the particles throughout the bend is strongly augmented. As the appearance of the particle concentration distribution within the bend (i.e. degree of segregation) is depending on the bend Stokes number, also the inter-particle collision frequency is somehow coupled to this characteristic non-dimensional number (i.e. particle

inertia) and of course depending on the overall loading ratio. In the case particles with a wide size distribution are conveyed also the so called impact efficiency becomes of importance. This means that once a small and large particle are on a collision trajectory, the small particle still might move around the larger collector particle with the relative velocity field and hence no collision occurs (Ho and Sommerfeld 2002, Sommerfeld and Lain 2009). In average this phenomenon reduces the collision frequency of inter-particle collisions (Ho and Sommerfeld 2005). In the following sections the influence of the particle phase properties and the elementary processes described above on the pneumatic conveying characteristics and the resulting pressure drop will be discussed.

Validation of the Computations

The modelling approach summarised above has been thoroughly validated for different pneumatic conveying systems, i.e. horizontal channel (Lain and Sommerfeld 2008, 2012 a) and a pipe systems within a vertical pipe (Lain and Sommerfeld 2010). In the following the validation is based on results for the 80 mm pipe system, obtained at several cross-sections in the vertical pipe by applying phase-Doppler anemometry (Huber and Sommerfeld 1994). The computational results are shown for both two-way and four-way coupling.

A comparison between measured and calculated profiles for the particle concentration and mean diameter development downstream of the bend exit is shown in Fig. 2. The first two profiles exhibit a very good agreement,

both in shape and magnitude. Further downstream however, the predictions still show a higher concentration near the outer wall (right hand side) than the measurements. Hence, in the experiments the rope was faster dispersed in the vertical pipe which is most probable the result of the observed fluctuating motion of the rope downstream of the bend exit. The profiles of the calculated particle number mean diameter show a remarkable good agreement with the measurements, particularly since this property is the result of the size segregation within the bend and requires a good prediction of the local particle size distributions. Only the first profile shows some larger deviations, indicating a somewhat stronger rebound of the larger particles in the predictions.

The predicted particle mean velocities (vertical component) and the associated particle rms-values are compared in Fig. 3. The mean velocities in the first two cross-sections are in reasonable good agreement, however, some larger deviations are found in the last profile, which is again associated with the differences in predicting the disintegration of the rope (Fig. 2), being most likely due to the rope fluctuations observed in the experiments. The predicted particle-phase rms values of the vertical velocity are in surprisingly good agreement with the measurements, as this property is affected by all relevant transport processes, especially the description of the turbulence seen by the particles.

As to be expected when neglecting inter-particle collisions, the rope behaviour in the vertical pipe cannot be predicted properly (see below) and consequently all the

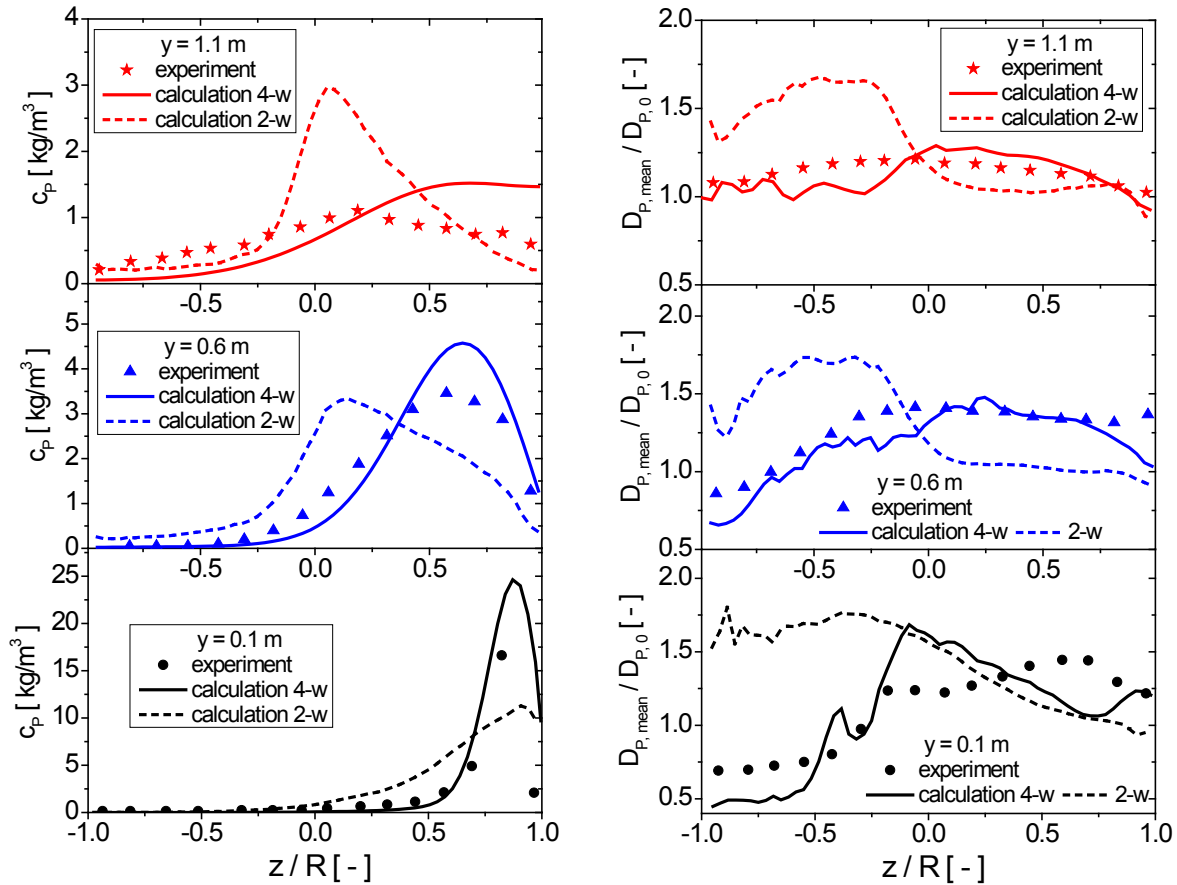


Figure 2: Profiles of particle concentration (left) and particle mean number diameter (right) downstream of the bend exit, comparison of calculations with experiments ($D = 80$ mm, $R_{\text{bend}} = 0.203$ m, $U_0 = 14$ m/s, $\eta = 0.5$, $\Delta\gamma = 10^\circ$, four-way coupling, particle size distribution $15 - 85$ μm , $St_{\text{bend}} = 0.076 - 2.445$).

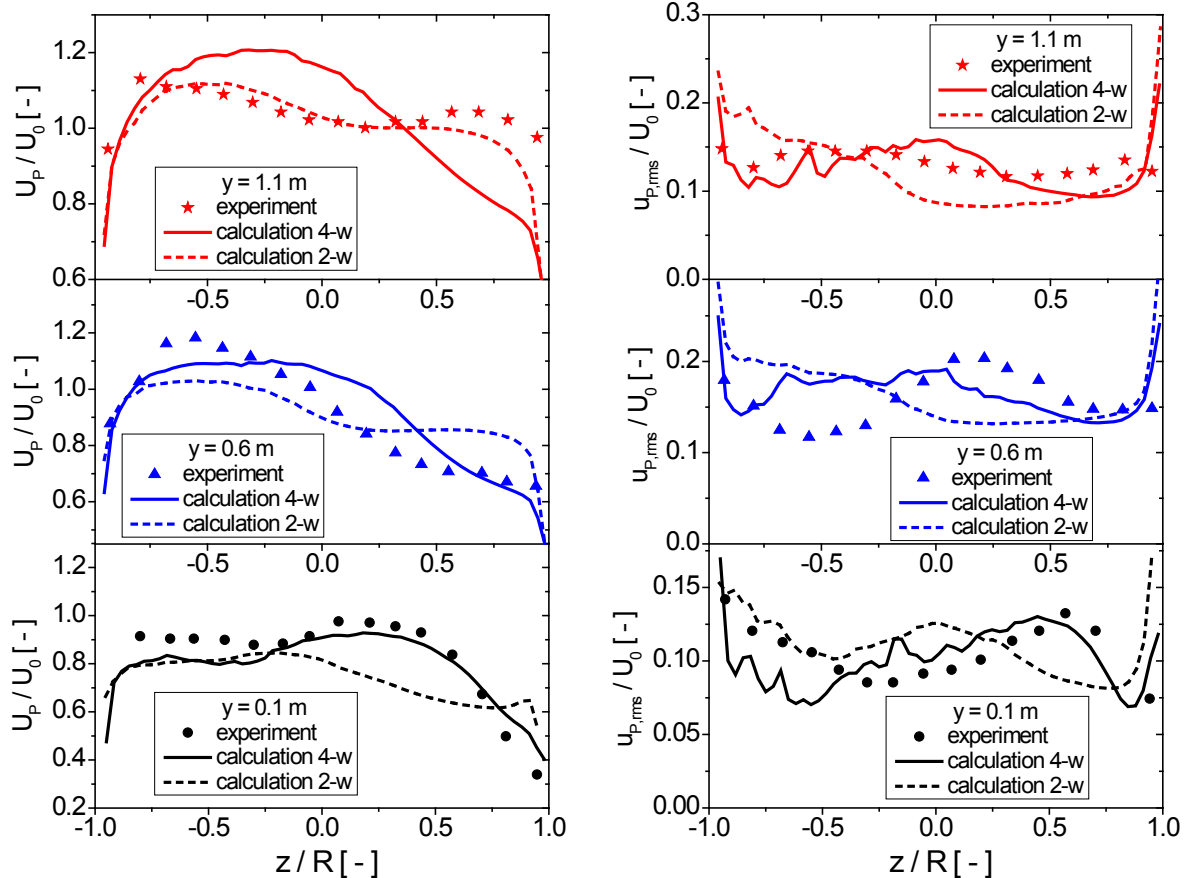


Figure 3: Profiles of vertical particle velocity (left) associated rms-value (right) downstream of the bend exit, comparison of calculations with experiments ($D = 80$ mm, $R_{\text{bend}} = 0.203$ m, $U_0 = 14$ m/s, $\eta = 0.5$, $\Delta\gamma = 10^\circ$, four-way coupling, particle size distribution $15 - 85$ μm , $St_{\text{bend}} = 0.076 - 2.445$).

other particle phase properties are also not correctly predicted. Here the particles may be reflected unhindered from the bend outer wall towards the pipe core yielding the highest particle concentrations near the core of the pipe after some distance from the bend exit (Fig. 2 left, $y = 0.6$ and 1.1 m). As a consequence of the higher inertia of large particles the particle mean diameter left of the pipe axis is remarkably over-predicted when not considering inter-particle collisions (Fig. 2 right).

Wall Roughness Effects

In order to decouple the problem first calculations are considered where only the effect of wall roughness is analysed by neglecting inter-particle collisions, i.e. conducting two-way coupled calculations for the case with particle size distribution from $15 - 85$ μm . For this case a *short inlet pipe of 1 m* is used, which results in an almost homogeneous concentration distribution at the bend inlet (Lain and Sommerfeld 2009, 2012 c). The degree of accumulation of particles at the bend outer wall depends strongly on wall roughness describing the rebound characteristics of the particles. Two degrees of roughness are considered, namely $\Delta\gamma = 1.5^\circ$ and 10° and the resulting computational results are compared with respect to the particle concentration distribution along horizontal pipe, bend and vertical pipe (Fig. 4 left). When entering the bend particles are first driven towards the bend outer wall mainly due to inertia and to some extent by the secondary flow. For small roughness, $\Delta\gamma = 1.5^\circ$, the particle rebound

is not very strong and consequently a quite dense rope is formed at the bend exit. However, in the third cross-section within the bend ($\theta = 60^\circ$) a small nose in the concentration distribution is visible caused by the focussing effect, i.e. particles reflected at a curved bend outer wall are bounced back towards the core of the pipe (Sommerfeld and Lain 2009). Finally, particles are only present near the outer wall of the pipe bend leaving the bend inner region and the core almost without solids (Fig. 4 upper block). Near the exit of the bend the particles are again rebound from the outer (right) wall towards the core of the pipe (focussing), yielding a strip of high concentration, which reaches after 1 m the pipe core. This high concentration region is barely dispersed until the exit of the vertical pipe.

The secondary flow structure developing in the bend and the vertical pipe is also shown in Fig. 4 (upper block, right) for the low roughness case without inter-particle collisions. As a result of the particle rebound from the outer bend wall, the particles are reflected back towards the pipe centre. The associated momentum transferred to the fluid by this focussing (Sommerfeld and Lain 2009) produces two new counter-rotating vortices which push the two secondary flow vortices produced in the bend towards the inner part of the pipe cross-section. Eventually four vortical structures of roughly equal size appear in the pipe cross-section. Thereby, a stem-like and later on mushroom-shaped region of high particle concentration is

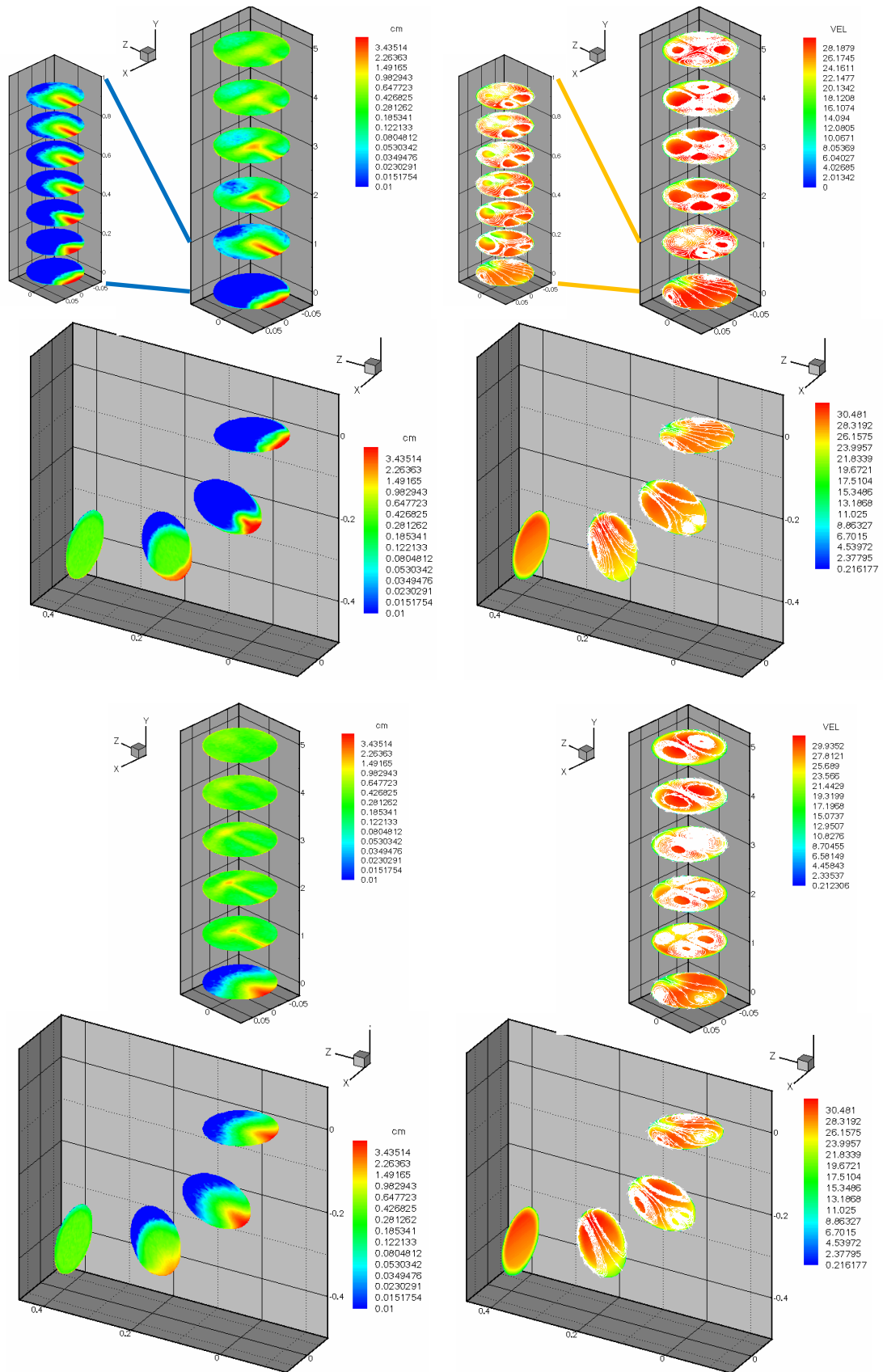


Figure 4: Development of cross-sectional distributions of particle concentration in kg/m^3 (left side) and absolute flow velocity in m/s (colour) as well as streamlines of the cross-sectional flow (white lines) (right block) for a particle-laden flow through the bend and vertical pipe; upper block: $\Delta\gamma = 1.5^\circ$, lower block: $\Delta\gamma = 10^\circ$ ($D = 150 \text{ mm}$, $U_0 = 27 \text{ m/s}$, $\eta = 0.3$, particle size distribution $15 - 85 \mu\text{m}$, two-way coupling, 1 m inlet pipe).

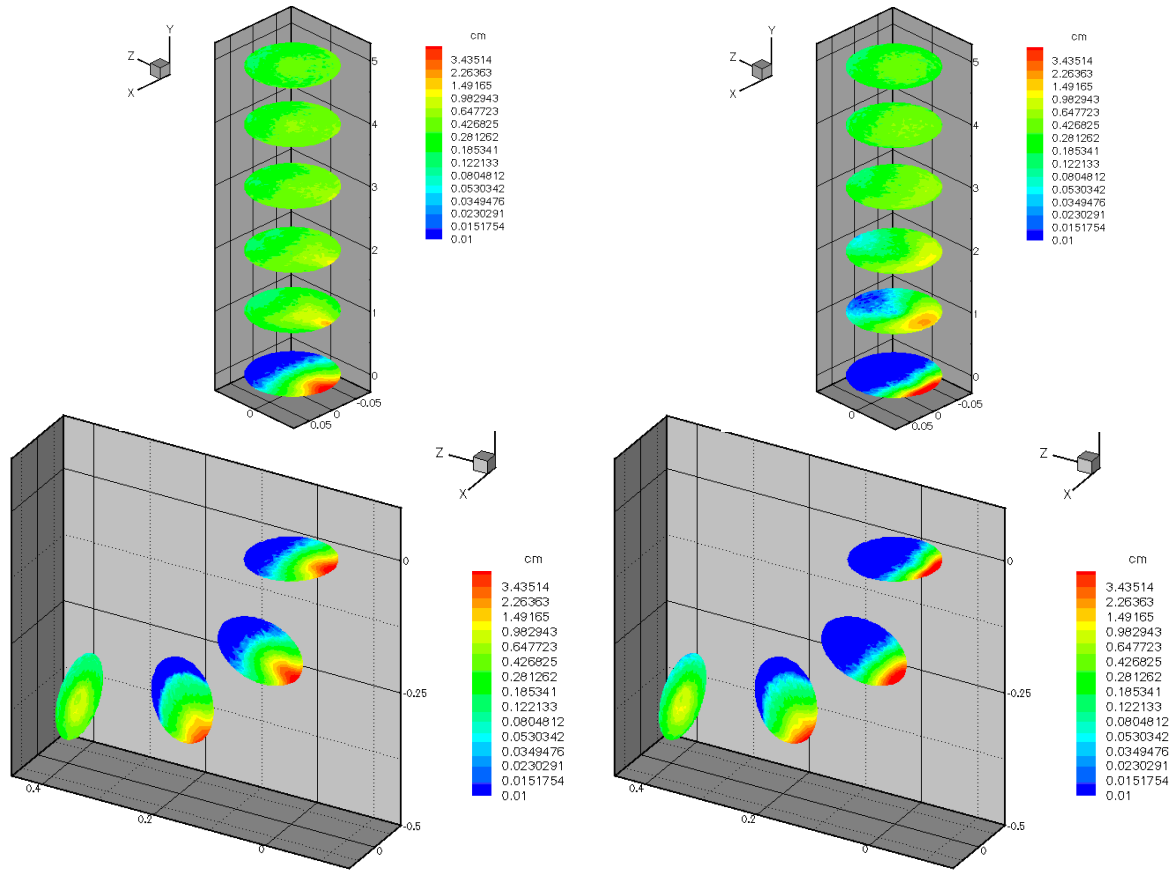


Figure 5: Cross-sectional distribution of particle concentration in kg/m^3 along bend and connecting vertical pipe: left) two-way coupling, right) four-way coupling ($D = 150$ mm, bend radius 2.54 pipe diameters, $U_{av} = 27$ m/s, $\eta = 0.3$, $\Delta\gamma = 10^\circ$, particle size distribution 15 – 85 μm).

developing in the vertical pipe (Fig. 4 upper block, left). Until the end of the vertical pipe element the regions of high particle concentration barely disappeared.

In the case of higher roughness, i.e. $\Delta\gamma = 10^\circ$, particles rebound from the bend outer wall are farther reflected back into the core region of the bend flow (Fig. 4 lower block). This behaviour is due to the shadow effect of wall roughness (Sommerfeld 2003, Lain and Sommerfeld 2008) implying that the rebound angle may become larger than the impact angle if this is relatively shallow (i.e. resulting in an averaged transfer of wall parallel particle momentum towards the transverse components). Hence, although a more or less dense rope is formed at the outer wall near the bend exit, the particles are distributed over a larger portion of the cross-section compared to the low roughness case (compare Fig. 4 left, upper and lower part). Only near the inner wall there are almost no particles (i.e. this region corresponds to about one third of the cross-section). The T-shaped regions of high particle concentration at 1 and 2 m downstream the bend exit are again associated with the focussing effect pushing the particles towards the pipe core. Within the bend already strong counter-rotating vortices develop due to the particle focussing, yielding in the initial portion of the vertical pipe four circulation cells in the pipe cross-section (Fig. 4 lower block right). As the strength of the particle induced circulation cells is quite high, the original circulation cells produced in the bend by the centrifuging effect are eventually completely entrapped (i.e. from about 3 m). Hence, at the end of the vertical pipe two circulation cells

are only present with a rotation opposite to that produced in a single-phase bend flow.

Influence of Inter-Particle Collisions

For the following results, the standard case with a 5 m horizontal pipe, a bend and a 5 m vertical pipe is considered and the particles have the size distribution specified in Table 2 (●). This implies that the particle laden flow entering the bend shows already a remarkable gravitational settling whereby the particle concentration at the inlet becomes non-symmetric. The result obtained for solely two-way coupled calculations is shown in Fig. 5 (left). Compared to the short inlet pipe (Fig. 4 upper block left) the focussing effect is much more distinctive whereby the particles are further rebound towards the pipe core. Hence already at the bend exit the particles are filling half the cross-section. In the vertical pipe this less concentrated rope is also dispersed much quicker. When inter-particle collisions are taken into account (i.e. four-way coupling), the particle rope developing in the bend is forced to be more concentrated and the particles are distributed in a smaller part of the cross-section near the outer wall of the bend compared to the result with only two-way coupling (compare Fig. 5 right and left). This is caused by collisions of particles moving into the bend with those rebounding from the bend outer wall. Hence, the rebound particles are “pushed” back towards the bend outer wall and will again collide with it. Also the re-dispersion of the particles in the vertical pipe section is hindered by inter-particle collisions. Instead a kind of detached closed rope

develops near the bend outer wall which moves upward and is only dispersed 3 m downstream the bend exit (Fig. 5).

Influence of Particle Size

In order to demonstrate the effect of the particle size on the conveying of the particles through the standard pipe configuration (5 m horizontal, bend and 5 m vertical) mono-sized particles of 40, 80 and 135 μm are considered. The particle behaviour in the different pipe elements may be first analysed by considering the different relevant transport mechanisms. In the horizontal pipe particle motion is governed by gravitational settling and the response to turbulence, i.e. gravitational settling may be balanced by turbulence if the particles are small enough. From the numerical calculations the integral length scale of turbulence is estimated to be $T_L = 0.16 k/\varepsilon = 10.3$ ms at the centre line of the pipe. With the Stokesian response time of the particles, turbulent Stokes numbers of 1.2, 4.8 and 13.7 are found for the three particle sizes. This shows that only the very small particles may be affected by turbulence. The other elementary process strongly affecting the particle behaviour in the horizontal pipe, are wall collisions, especially for rough walls and the involved shadow effect (Sommerfeld and Huber 1999). Particle-wall collisions become of importance if their response distance (i.e. product of particle response time and terminal velocity) becomes larger than the dimension of the confinement (Sommerfeld et al. 2008), here the pipe diameter:

$$D < \lambda_p = \frac{\rho_p D_p^2}{18 \mu} V_s \quad (6)$$

The particle response distance for the three particle diameters is: 1.5, 23.9 and 194.0 mm, respectively. This clearly demonstrates that the small particles are not strongly influenced by wall collisions including roughness. Hence, due to the partial balance between gravitational settling and turbulence these particles (40 μm) are more or less homogeneously distributed at the end of the horizontal pipe (Fig. 6). The middle sized particles (80 μm) are stronger rebound towards the pipe core, which is yet enhanced by the shadow effect, and hence a clear concentration maximum is arising around the core (Fig. 7). As the response distance of the large particles (135 μm) is considerably greater than the pipe diameter (see Table 2) they will eventually bounce from wall to wall (Sommerfeld 2003) with the result of an almost constant concentration distribution at the end of the horizontal pipe, i.e. the entrance of the bend (Fig. 8).

Within the bend the segregation of the particles is first affected by their ability to follow the flow deflection, characterised by the bend Stokes number, which for the considered particle sizes is 0.557, 2.228 and 6.344, respectively. Consequently, all considered particle sizes are governed by inertial segregation (centrifuging) since the Stokes number is not much smaller than 1 and hence are driven towards the bend outer wall (i.e. right hand side of the graphs). Secondly the development of the

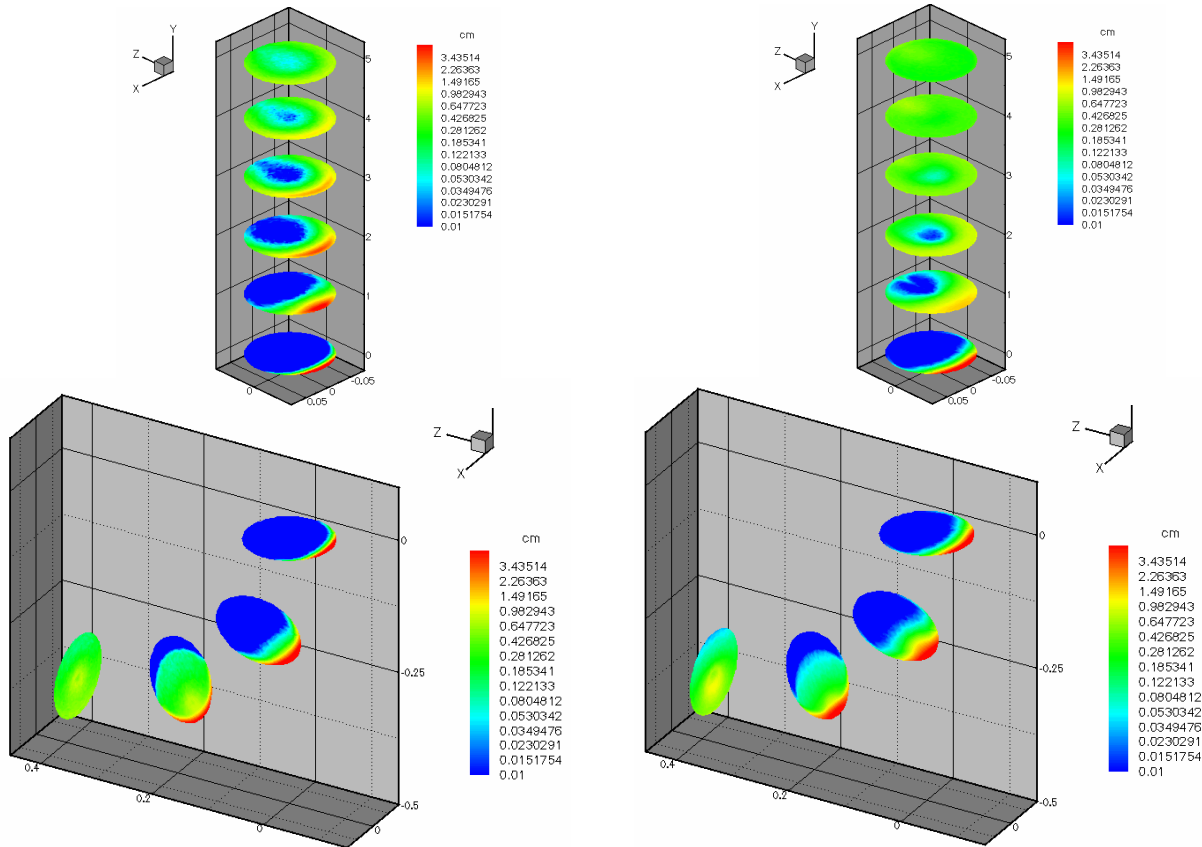


Figure 6: Cross-sectional distribution of particle concentration in kg/m^3 along bend and vertical pipe ($D = 150$ mm, $U_0 = 27$ m/s, $\eta = 0.3$, $\Delta\gamma = 10^\circ$, four-way coupling, mono-sized 40 μm)

Figure 7: Cross-sectional distribution of particle concentration in kg/m^3 along bend and vertical pipe ($D = 150$ mm, $U_0 = 27$ m/s, $\eta = 0.3$, $\Delta\gamma = 10^\circ$, four-way coupling, mono-sized 80 μm)

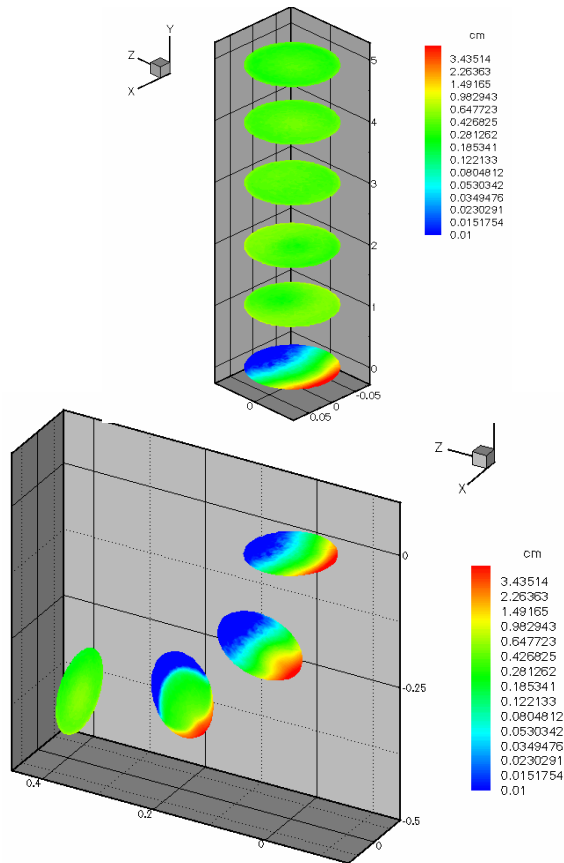


Figure 8: Cross-sectional distribution of particle concentration in kg/m^3 along bend and vertical pipe ($D = 150 \text{ mm}$, $U_0 = 27 \text{ m/s}$, $\eta = 0.3$, $\Delta\gamma = 10^\circ$, four-way coupling, mono-sized $135 \mu\text{m}$).

concentration distribution within the bend is affected by particle-wall collisions including wall roughness effects. As shown above, the rebound distance of the small particles is also very small and they are more easily carried by the flow along the bend. Consequently, a narrow dense rope is formed for the $40 \mu\text{m}$ -particles (Fig. 6). Also note that the particles being rebound are again pushed towards the wall by collisions with the oncoming particles (see above). In the vertical pipe the disintegration of the powder rope is very slow and mainly resulting from the secondary flow, gradually transporting the particle along the lateral walls to the inner wall of the vertical pipe. Note that in this case the secondary flow cannot be strongly affected by the particles as the rope remains very narrow whereas the secondary flow has only two circulation cells moving outward towards the right in the core region and backward along the lateral pipe walls. As a result, in the core of the pipe a particle-free region develops and is maintained up to the vertical pipe exit (Fig. 6).

Regarding the larger $80 \mu\text{m}$ -particles, the observed transport phenomena are very similar with the only difference that the rope developing in the bend is wider and the maximum concentration is lower (Fig. 7). This is stemming from the larger response distance of these particles and the farther rebound after a wall collision within the bend, although oncoming particles collide with rebound particles. In the 3rd cross-section within the bend ($\theta = 60^\circ$) one can perceive the focussing effect whereby the particles are bounced back towards the pipe core due

to the curved bend outer wall (i.e. a concentration maximum is observed in this region). In the vertical pipe the particles are better entrained in the secondary flow due to their faster rebound and a nice concentration structure is seen in the second cross-section (i.e. 1 m downstream of the bend exit) where the particles clearly mark the secondary flow structure, which in this case has only two circulation cells (not shown).

The largest particles considered, are very inertial (i.e. bend Stokes number 6.344) and hence are rebound at the bend outer wall almost completely towards the inner wall of the bend whereby a wide rope is formed and the particle free region is only about 33 % of the pipe cross-section (Fig. 8). Also here the focussing effect is clearly seen. In the vertical pipe the strong rebound of the particle close to the end of the bend and their large inertia results in an almost homogeneous concentration distribution already 1 m downstream of the bend exit.

The development of the particle concentration distribution along horizontal pipe, bend and vertical pipe may be characterised in summary through a non-dimensional segregation parameter which is a weighted average of the local particle concentration with respect to the radial displacement of the control volume from the pipe centre within each cross-section:

$$R_{c,\max} = \frac{1}{c_{av} R_o V_{\text{cross}}} \sum_1^{N_i} c_i r_i V_i \quad (7)$$

where c_i is the particle concentration in the computational cell, r_i is the vector indicating the centre of the cell and V_i is its volume. The product of these three quantities is summarised over all control volumes in one cross-section and divided by the average concentration, c_{av} , the pipe radius R_o and the total volume of the slice V_{cross} . In the present work r_i is defined to be positive if the control volume is located below or to the right of the centre line. Hence, the segregation parameter varies in the range $-1 < R_{c,\max} < 1$. This segregation parameter is plotted versus the non-dimensional distance along the pipe centre line s/D (Fig. 9), where D is the pipe diameter.

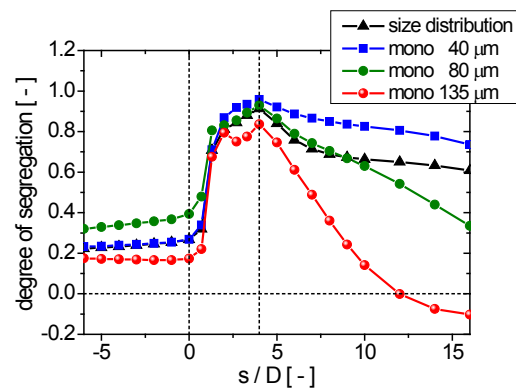


Figure 9: Non-dimensional segregation parameter along the pipe system for the cases 1 to 4 in Table 2 (size distribution Fig. 4 right, mono-sized $40 \mu\text{m}$ Fig. 5, mono-sized $80 \mu\text{m}$ Fig. 6, mono-sized $135 \mu\text{m}$ Fig. 7 ($D = 150 \text{ mm}$, $U_0 = 27 \text{ m/s}$, $\eta = 0.3$, $\Delta\gamma = 10^\circ$, bend radius 2.54 pipe diameters, four-way coupling).

In the horizontal pipe ($s/D < 0$) gravitational settling can be clearly identified since $R_{c,\max}$ is larger than zero. The strongest gravitational settling is found for the $80 \mu\text{m}$ -particles and both smaller and larger particles are more

homogeneously distributed; the small particles through turbulence and the large once due to inertia and wall collisions (Fig. 9). Within the bend the densest rope is formed by the 40 μm -particles which is hardly dispersed in the vertical pipe. The largest considered particles are very quickly dispersed in the vertical pipe and beyond $s/D = 12$ the concentration maximum moves even towards the inner wall side (i.e. negative $R_{c,\text{max}}$). The segregation parameter for the particle with size distribution in the vertical pipe shows clearly two slopes. Initially the location of the concentration maximum is determined by the larger particles in the spectrum and then beyond $s/D > 7$ by the small particles (Fig. 9).

The development of the particle concentration throughout the bend is also correlated to the cross-sectional average of the normalised particle fluctuating energy (Fig. 10 top). The values for the 40 μm -particles are very low, even smaller than the fluid fluctuation (Fig. 10 bottom). Towards the end of the bend the fluctuation is yet further decreasing and then within the vertical pipe begins to rise again. These low values are associated with the densest regions of the dust rope where the particles are entrapped within the rope due to inter-particle collisions and the fluctuation is damped. With increasing particle size the fluctuation energy of the particle is then continuously increasing throughout the entire pipe system and becomes larger than the values of the fluid, being a result of the raising inertial behaviour of the particles. Within the bend a drastic growth is observed especially for the 80 μm -particles, caused by the stronger rebound of the particles from the bend outer wall. From the middle region of the

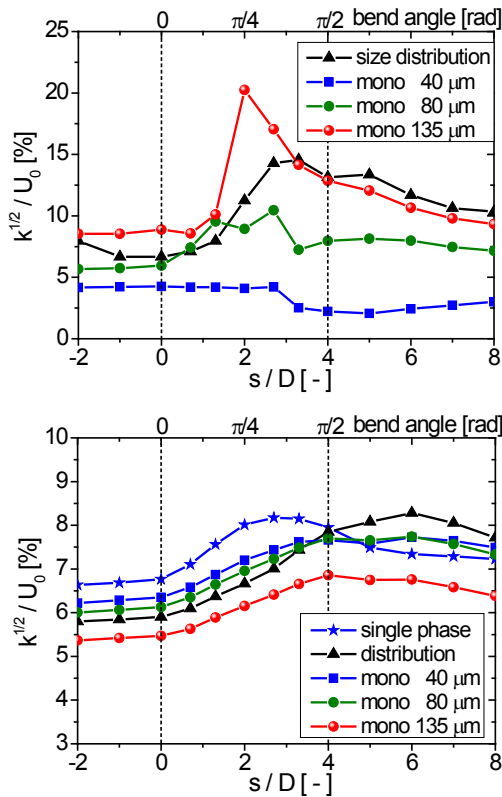


Figure 10: Fluctuating energy along the extended pipe bend; top) particle-phase, bottom) gas-phase ($D = 150$ mm, $U_0 = 27$ m/s, $\eta = 0.3$, $\Delta\gamma = 10^\circ$, bend radius 2.54 pipe diameters, four-way coupling, different particle sizes).

bend the particle velocity fluctuation is continuously decreasing since the deflection of the particle stream is mostly completed. The particle fluctuations for the size distribution are lying between those of the larger mono-sized particles; however rise beyond their values in the vertical pipe as a consequence of the different response of particles in a wide size spectrum (Sommerfeld 1990).

Cross-sectional averages of gas phase fluctuation along the bend with inlet and outlet sections are shown in Fig. 10. The gas-phase fluctuating velocity is remarkably reduced by the particles compared to the single-phase flow in the horizontal pipe section and also within the bend until its outlet. The turbulence dissipation is continuously increasing with growing particle size as a consequence of coupling, i.e. growing of the particle phase source terms in the kinetic energy transport equation. Within the vertical pipe the single-phase turbulent kinetic energy is reduced and that in the two-phase situation remains initially almost constant due to an additional production of turbulence at the edge of the dust rope developing in the bend which persists at least up to 1 m downstream of the bend exit. Thereby the two-phase fluid fluctuation becomes larger than for the single-phase flow except for the mono-sized 135 μm -particles, as they are homogeneously distributed.

Influence of Mass Loading

The influence of particle mass loading on the particle concentration distribution throughout the standard pipe system is analysed for the case with particle size distribution (case 1 in Table 2). The result for a mass loading of 0.3 with consideration of inter-particle collisions is shown in Fig. 5 (right). In the case of a mass loading of 1.0 several phenomena may be observed. First the gravitational settling of the particle in the horizontal pipe is more pronounced (Fig. 11). The development of the concentration distribution within the bend is very similar for both loadings, except regarding the magnitude. The regions occupied by the particle have almost the same shape. For the high mass loading the concentrated rope formed within the bend is not disintegrating within the vertical pipe, however is expanding laterally up to the side walls. This is caused by the secondary flow which also in this high loading case is almost unaltered by the particles as the rope remains rather concentrated. This is an indication for the fact that the particles are entrapped within the rope due to inter-particle collisions, i.e. the mean free path between particle collisions is remarkably reduced due to the high concentration so that the particle are not able to move out of the rope.

Influence of Orientation

Besides the above studied pipe configuration (i.e. horizontal to vertical) numerous other more complex geometries exist. Here a horizontal arrangement is considered (i.e. 5 m horizontal pipe, bend and 5 m horizontal pipe). In such a situation the gravity vector is perpendicular to the plane of the pipes. As a result of gravitational settling in the horizontal pipe the rope enters the bend at the side wall and is driven due to the centrifugal force to the bend outer wall (right hand side), see Fig. 12. Thereby a rotational momentum is transmitted to the rope and this left rotation is maintained throughout the connecting horizontal pipe. Hence the angular location of the rope is -90° at the bend inlet, 0° at the bend outlet and $+90^\circ$ at the end of the connecting horizontal pipe, i.e. after 5 m conveying distance. The secondary flow

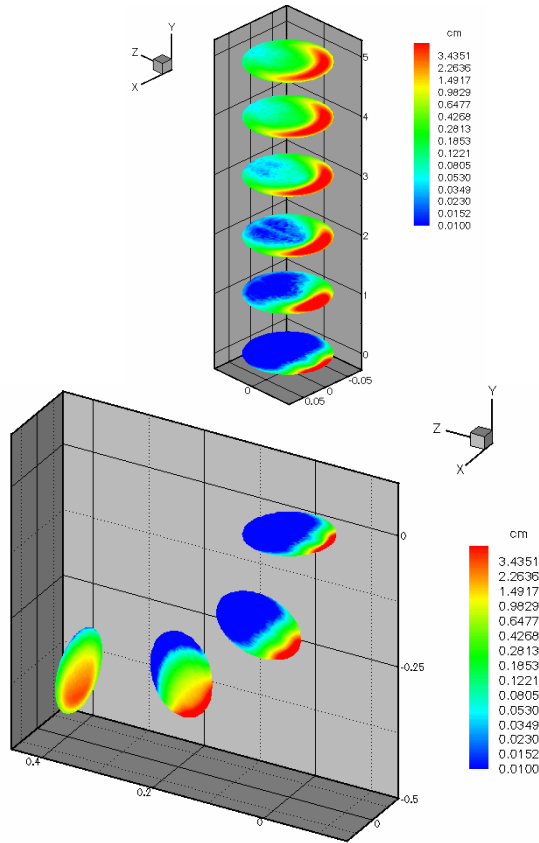


Figure 11: Cross-sectional distribution of particle concentration in kg/m^3 along bend and vertical pipe ($D = 150$ mm, $U_0 = 27$ m/s, $\eta = 1.0$, $\Delta\gamma = 10^\circ$, particle size distribution $15 - 85$ μm , four-way coupling).

developing in this situation within the bend is first impressed by the centrifuging effects of the gas flow, showing a similar structure as in a single phase flow. In the horizontal pipe the two circulation cells begin then to rotate with the dust rope and at the end a closed single cell is formed (not shown).

Analysis of Pressure Drop

For all the cases discussed above also the pressure drop in the entire pipe system, as well as that in the individual elements were determined from the calculations (Table 3). In pneumatic conveying the pressure drop is composed of the single-phase pressure drop and the additional pressure drop due to the presence of the particle. This additional pressure drop of course depends on the mass loading and results from the following effects (Siegel 1991):

- Particle-wall collisions (often termed particle wall friction) which is present in all pipe elements and constitutes the main contribution.
- Particle re-acceleration after a redirection of the two-phase flow, as for example in a bend, resulting from wall collisions and inter-particle collisions influencing wall collision rates; this effectively reduces the particle velocity at the end of such a pipe element remarkably (see Fig. 3 left).
- Particle lifting in vertical pipe elements; hence the pressure drop in the vertical pipe has the largest value.

From the results presented in Table 3 the following results are obtained:

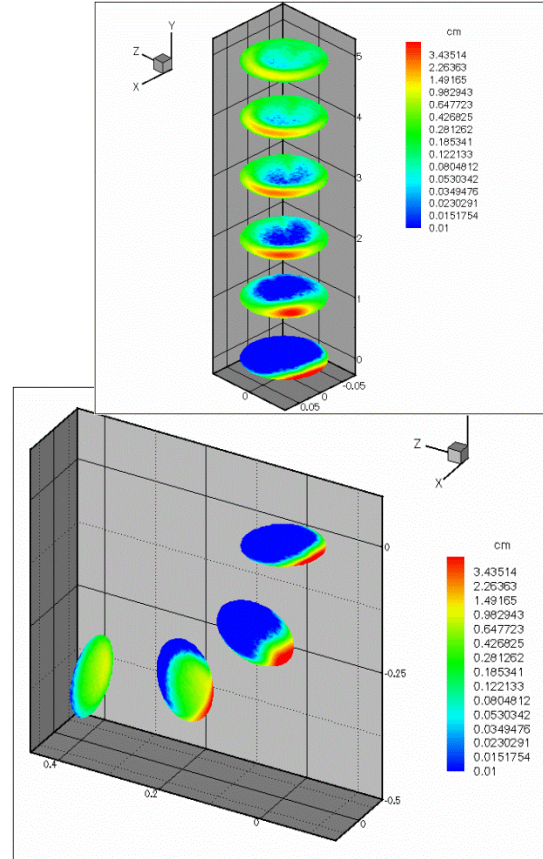


Figure 12: Cross-sectional distribution of particle concentration in kg/m^3 along bend and horizontal pipe ($D = 150$ mm, $U_0 = 27$ m/s, $\eta = 0.3$, $\Delta\gamma = 10^\circ$, particle size distribution $15 - 85$ μm , four-way coupling).

- Increasing wall roughness enhances wall collisions (through the shadow effect) and hence particle-phase pressure drop due to the required re-acceleration of the particles by the fluid.
- Naturally the pressure drop is increased with the mass loading of the particles.
- When increasing the size of mono-disperse particles in the range considered here (i.e. from 40 to 135 μm), the particle response characteristics goes from partly responsive to very inertial (see Table 2), thus the wall collision frequency and the pressure drop increase.
- The system with the particle size distribution ($15 - 85$ μm) shows the highest pressure drop.

Case	Δp total [Pa]	Δp hor. [Pa]	Δp bend [Pa]	Δp vertical [Pa]
Single phase	556	231	92	233
① $\eta = 0.3$	803	281	147	374
① $\eta = 1.0$	902	361	139	402
① $\Delta\gamma = 1.5^\circ$	756	262	132	362
② 40 μm	656	251	113	295
③ 80 μm	716	260	125	331
④ 135 μm	761	273	135	353
⑤ $30 + 60$ μm	748	276	142	330

Table 3: Calculated pressure drop across the different pipe elements for the various conditions considered ($D = 150$ mm, $U_0 = 27$ m/s, $\eta = 0.3$ (except for case $\eta = 1.0$), $\Delta\gamma = 10^\circ$ (except for case with $\Delta\gamma = 1.5^\circ$), bend radius 2.54 pipe diameters, four-way coupling).

CONCLUSION

By applying the Euler/Lagrange approach in combination with the k- ϵ turbulence model and considering full two-way coupling as well as all relevant elementary processes for calculating particle transport dilute phase pneumatic conveying through a horizontal pipe, a bend and a vertical pipe was analysed in detail. It was demonstrated that both particle-wall collisions, respecting roughness and inter-particle collisions have a remarkable effect on the developing two-phase flow structure, especially the particle concentration distribution. For characterising the location of maximum particle concentration a weighted segregation parameter was introduced. Due to inter-particle collisions, the particles tend to be trapped within the dust rope forming in the bend due to centrifugal effects. Thereby, especially at higher mass loading the developing rope is not disintegrated in the vertical pipe. Moreover, the particle size and their resulting response behaviour have a remarkable effect on the rope development and disintegration. For particles with bend Stokes numbers around one, a rather dense rope is formed in the bend which is also hard to be disintegrated in the vertical pipe. For very inertial particles their distribution at the end of the vertical pipe is very homogeneous. In the case of two horizontal pipes connected by a bend a rotation of the dust rope formed within the bend is induced. At the end of the second horizontal pipe the dust rope however still exists and hence not disintegrated completely. These findings are of significance whenever at the end of a pneumatic conveying system a homogeneous powder distribution is required, as for example in the case of pulverised coal dust conveying in a power plant.

REFERENCES

- HO, C.A. and SOMMERFELD, M. (2002) Modelling of micro-particle agglomeration in turbulent flow. *Chemical Engineering Science*, **57**, 3073-3084.
- HO, C.A. und SOMMERFELD, M. (2005) Numerische Berechnung der Staubabscheidung im Gaszyklon unter Berücksichtigung der Partikelagglomeration. *Chemie Ingenieur Technik*, **77**, 282-290.
- HUBER, N. and SOMMERFELD, M. (1994) Characterization of the cross-sectional particle concentration distribution in pneumatic conveying systems. *Powder Technology*, **79**, 191-210.
- HUBER, N. and SOMMERFELD, M. (1998) Modelling and numerical calculation of dilute-phase pneumatic conveying in pipe systems. *Powder Technology*, **99**, 90-101.
- KOHNNEN, G., RÜGER, M. and SOMMERFELD, M. (1994) Convergence behaviour for numerical calculations by the Euler/Lagrange method for strongly coupled phases. *Numerical Methods in Multiphase Flows 1994*, (Eds. C.T. Crowe et al.), ASME Fluids Engineering Division Summer Meeting, Lake Tahoe, U.S.A., FED-Vol. **185**, 191-202.
- LAIN, S., SOMMERFELD, M. and KUSSIN, J. (2002) Experimental studies and modelling of four-way coupling in particle-laden horizontal channel flow. *Int. Journal of Heat and Fluid Flow*, **23**, 647-656.
- LAIN, S. and SOMMERFELD, M. (2008) Euler/Lagrange computations of pneumatic conveying in a horizontal channel with different wall roughness. *Powder Technology*, **184**, 76-88.
- LAIN, S. and SOMMERFELD, M. (2009) Structure and Pressure drop in particle-laden gas flow through a pipe bend: A numerical analysis by the Euler/Lagrange approach. *Proceedings of the ASME Fluids Engineering Division Summer Meeting*, Vail, Colorado, Paper No. FEDSM2009-78090.
- LAIN, S. and SOMMERFELD, M. (2010) Euler/Lagrange computations of particle-laden gas flow in pneumatic conveying systems. *CD-ROM Proceedings 7th International Conference on Multiphase Flow, ICMF2010*, Tampa, FL USA, May 30. – June 4.
- LAIN, S. and SOMMERFELD, M. (2011) Numerical analysis of a pneumatic conveying system consisting of a horizontal pipe, 90°-bend and vertical pipe. *12th Int. Conf. on Multiphase Flow in Industrial Plants*. Paper No. 141, Ischia (Napoli), Italy September 21-23.
- LAIN, S. and SOMMERFELD, M. (2012 a) Numerical calculation of pneumatic conveying in horizontal channels and pipes: Detailed analysis of conveying behaviour. *Int. J. of Multiphase Flow*, **39**, 105–120.
- LAIN, S. and SOMMERFELD, M. (2012 b) Influence of geometrical and operational conditions on the performance of pneumatic conveying systems: A numerical study by the Euler-Lagrange approach. *9th International ERCOFTAC Symposium ETMM9*, Thessaloniki, Greece, 6. – 8. June 2012.
- LAÍN, S. and SOMMERFELD, M. (2012 c) Characterisation of pneumatic conveying systems using the Euler/Lagrange approach, Submitted to *Powder Technology*, August 2012
- SIEGEL, W. (1991) *Pneumatische Förderung: Grundlagen, Auslegung, Anlagenbau, Betrieb*. Vogel Verlag, Würzburg.
- SOMMERFELD, M. (1990) Particle dispersion in turbulent flow: The effect of particle size distribution. *Part. and Part. Systems Characterization*, **7**, 209-220.
- SOMMERFELD, M. (1992) Modelling of particle/wall collisions in confined gas-particle flows. *Int. J. Multiphase Flow*, **18**, 905-926.
- SOMMERFELD, M., KOHNEN, G., and RÜGER, M. (1993) Some open questions and inconsistencies of Lagrangian dispersion models. *Proc. 9th Symp. on Turbulent Shear Flows*, Kyoto, Japan, paper 15-1.
- SOMMERFELD, M. (1998) Modelling and numerical calculation of turbulent gas-solid flows with the Euler/Lagrange approach. *KONA (Powder and Particle)*, **16**, 194-206.
- SOMMERFELD, M. and HUBER, N. (1999) Experimental analysis and modelling of particle-wall collisions. *Int. J. of Multiphase Flow*, **25**, 1457-1489.
- SOMMERFELD, M. (2001) Validation of a stochastic Lagrangian modelling approach for inter-particle collisions in homogeneous isotropic turbulence. *Int. J. of Multiphase Flows*, **27**, 1828-1858.
- SOMMERFELD, M., (2003) Analysis of collision effects for turbulent gas-particle flow in a horizontal channel: Part I. Particle transport". *Int. J. Multiphase Flow*, **29**, 675-699.
- SOMMERFELD, M., VAN WACHEM, B. and OLIEMANS, R. (2008) *Best Practice Guidelines for Computational Fluid Dynamics of Dispersed Multiphase Flows*. ERCOFTAC, Brussels, ISBN 978-91-633-3564-8.
- SOMMERFELD, M. and LAIN, S. (2009) From elementary processes to the numerical prediction of industrial particle-laden flows. *Multiphase Science and Technology*, **21**, 123 – 140.